Stochastic transformations of multi-rhythmic dynamics and order–chaos transitions in a discrete 2D model

Cite as: Chaos **31**, 063121 (2021); doi: 10.1063/5.0054679
Submitted: 21 April 2021 · Accepted: 31 May 2021 ·
Published Online: 15 June 2021

Ivan Tsvetkov, Irina Bashkirtseva,[a] and Lev Ryashko

AFFILIATIONS

Department of Theoretical and Mathematical Physics, Ural Federal University, Lenina 51, Ekaterinburg 620000, Russia

Note: This paper is part of the Focus Issue, In Memory of Vadim S. Anishchenko: Statistical Physics and Nonlinear Dynamics of Complex Systems.

[a]**Author to whom correspondence should be addressed:** Irina.Bashkirtseva@urfu.ru

ABSTRACT

A problem of the analysis of stochastic effects in multirhythmic nonlinear systems is investigated on the basis of the conceptual neuron map-based model proposed by Rulkov. A parameter zone with diverse scenarios of the coexistence of oscillatory regimes, both spiking and bursting, was revealed and studied. Noise-induced transitions between basins of periodic attractors are analyzed parametrically by statistics extracted from numerical simulations and by a theoretical approach using the stochastic sensitivity technique. Chaos–order transformations of dynamics caused by random forcing are discussed.

Rhythmicity is known to be a key common feature of all living systems. The study of the mechanisms of generation and transformation of oscillatory modes is a challenging problem of modern nonlinear dynamics. The complex behavior of some systems is due to the fact that oscillatory modes with different spatial and frequency characteristics coexist in them. In the present paper, we study a phenomenon of multirhythmicity on the basis of the conceptual Rulkov model of neural activity. In a certain range of parameters, this model exhibits a coexistence of oscillatory modes in the form of tonic spiking and bursting. In multirhythmic systems, random disturbances essentially complicate dynamics and cause transitions from one rhythm to another. We study the mechanisms of these effects and reveal some kind of "stochastic preference" by the mathematical approach based on the analysis of the sensitivity of periodic attractors to noise. It is shown that the noise-induced transitions between different rhythms are accompanied by chaos–order transformations.

I. INTRODUCTION

In the development of the theory of complex nonlinear processes, models of neural activity play an important role.[1,2] Various oscillatory regimes in the form of spiking and bursting are key intrinsic features of the behavior of neurons.[3] In the elucidation of the internal mechanisms of the transformation of the oscillatory activity of both individual neurons and neural systems, FitzHugh–Nagumo,[4–6] Morris–Lecar,[7] Hindmarsh–Rose,[8–10] and Hodgkin–Huxley[11–13] models in the form of differential equations are actively used. Among map-based neuron models, the system proposed by Rulkov is well known.[14–17] This conceptual two-dimensional model simulates features of the neuron behavior, such as quiescence, tonic spiking, and bursting. On the basis of this model, intriguing phenomena of Canard explosion and chaotic excitement were investigated.[18–20] The Rulkov model is actively used in the study of complex dynamics of neural networks.[21–25]

Multistability is one of the reasons that significantly complicate the behavior of dynamical systems.[26] It is well known that in nonlinear systems, even weak inevitable random disturbances can cause new diverse dynamical regimes, which are not observed in initial unforced models.[5,27–33] Nowadays, a phenomenon of multirhythmicity, namely, the coexistence of multiple oscillations with different spatial and frequency features, is of special interest. Many real systems are characterized by birhythmicity with the coexistence of two periodic attractors, both regular and chaotic (see, e.g., Refs. 34–36). A problem of the switching between multiple periodic attractors was studied in Refs. 37–39.

In the present paper, for the study of stochastic effects in multirhythmic nonlinear systems, we use the two-dimensional Rulkov model with discontinuous map.[14] In this model, a parameter zone with diverse scenarios of multirhythmicity was revealed.

In Sec. II, we describe dynamical regimes in the Rulkov model in the parameter zone of the coexistence of periodic attractors: spiking cycles of various periods and bursts. It is shown how a degree of multirhythmicity changes with the variation of the control parameter.

Section III aims to study how random disturbances affect the system dynamics in the presence of multirhythmicity. Stochastic transitions between coexisting cycles and the phenomenon of "noise-induced preference" are identified numerically and investigated analytically by the method of stochastic sensitivity. We show that the probabilistic mechanisms of these stochastic effects can be clarified by the analysis of the mutual arrangement of basins of attraction and confidence ellipses.[40] This technique is also applied to the analysis of stochastic generation and suppression of bursting-type oscillations. Analyzing Lyapunov exponents, we show that these deformations of stochastic dynamics are accompanied by order–chaos transformations.

II. DETERMINISTIC MODEL

In the present paper, as a deterministic skeleton, we use the known conceptual neuron model with discontinuous map,[14]

$$\begin{aligned} x_{t+1} &= f(x_t, y_t), \\ y_{t+1} &= y_t - \mu(x_t - \sigma + 1), \end{aligned} \tag{1}$$

where

$$f(x,y) = \begin{cases} \dfrac{\alpha}{1-x} + y, & x \le 0, \\ \alpha + y, & 0 < x < \alpha + y, \\ -1, & x \ge \alpha + y. \end{cases}$$

When the parameter μ is small, the gating variable y is slow whereas the variable x, replicating the membrane voltage, is fast. In Ref. 15, the bifurcation analysis of this slow–fast system for $\mu \to 0$ is presented.

System (1) possesses the equilibrium $E(\bar{x}, \bar{y})$, where $\bar{x} = \sigma - 1$, $\bar{y} = \bar{x} - \frac{\alpha}{1-\bar{x}}$. This equilibrium is stable for $\alpha < \alpha_1 = (1-\mu)(2-\sigma)^2$. In the present paper, we fix $\mu = 0.001$ and $\sigma = 0.6$, so $\alpha_1 = 1.958\,04$. For $\alpha > \alpha_1$, system (1) exhibits a phenomenon of multi-rhythmicity with the wide diversity of the coexisting periodic attractors. As the parameter α passes the bifurcation point $\alpha_2 = 7.6657$, a regime of bursting oscillations appears. So, system (1) models three key regimes of neuronal dynamics: quiescence, tonic spiking, and bursting.

The bifurcation diagram of system (1) vs parameter α is shown in Fig. 1 where by solid lines, we plot the extrema of x-coordinates of attractors.

Let us consider some examples of the system attractors for $\alpha > \alpha_1$. In Fig. 2, we show how oscillatory behavior changes as the parameter α moves away from the bifurcation point α_1. In the left panel, coexisting discrete cycles are plotted. In the middle and right panels, we show the time series for x- and y-coordinates by the same colors as the colors of cycles.

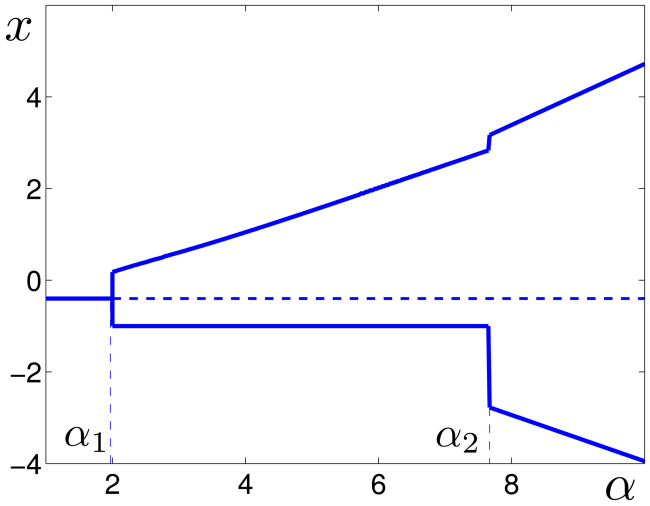

FIG. 1. Bifurcation diagram of system (1) vs α. Here, by solid lines, we plot extrema of x-coordinates of attractors. Bifurcation values are $\alpha_1 = 1.958\,04$ and $\alpha_2 = 7.6657$.

For $\alpha = 2$ [see Fig. 2(a)] that is close to $\alpha_1 = 1.958\,04$, system (1) exhibits 24 coexisting discrete cycles with periods ranging from 18 (green) to 41 (red).

For $\alpha = 3$ [see Fig. 2(b)], five discrete cycles coexist in system (1). Their periods change from 8 (blue) to 12 (red).

For $\alpha = 7$ [see Fig. 2(c)], three discrete cycles coexist with periods 9 (blue), 10 (green), and 11 (red).

For $\alpha = 7.5$ [see Fig. 2(d)], one can see two coexisting discrete cycles with periods 10 (blue) and 11 (red).

For $\alpha = 8$ [see Fig. 2(e)], system (1) has one 10-cycle.

So, as the parameter α moves right from α_1, the number of coexisting discrete cycles consequentially decreases [see Fig. 2(f)]. Note that these cycles describe the neuronal regime of tonic spiking.

When the parameter α passes the value α_2 from left to right, a type of the multi-rhythmicity qualitatively changes: in system (1), along with the tonic spiking, bursting oscillations appear.

An example of the coexistence of two cycles of periods 10 (green) and 11 (red) with the burst (blue) is shown in Fig. 3 for $\alpha = 7.7$. Details of initial and final spikes in the burst can be seen in Fig. 3(c). Here, the first spike has a period of four whereas the last one is 13-periodic.

In Sec. III, we explore how noise affects such multi-rhythmic dynamics.

III. STOCHASTIC MODEL

To analyze noise-induced phenomena, we will consider the following stochastic model:

$$\begin{aligned} x_{t+1} &= f(x_t, y_t) + \varepsilon\xi_t, \\ y_{t+1} &= y_t - \mu(x_t - \sigma + 1), \end{aligned} \tag{2}$$

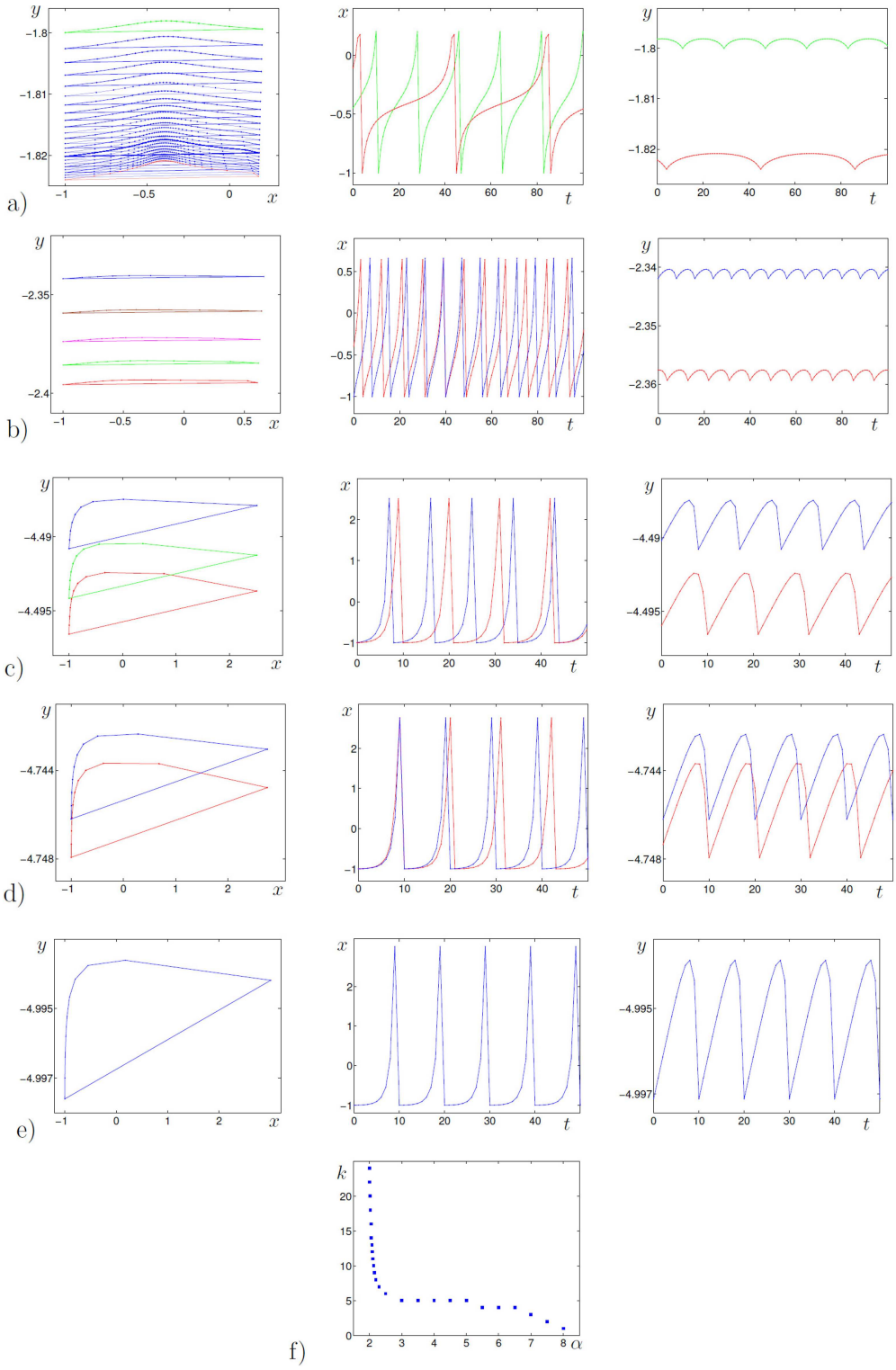

FIG. 2. Cycles and corresponding time series for the deterministic system (1) with (a) $\alpha = 2$, (b) $\alpha = 3$, (c) $\alpha = 7$, (d) $\alpha = 7.5$, and (e) $\alpha = 8$. In (f), the number of coexisting cycles vs parameter α is shown.

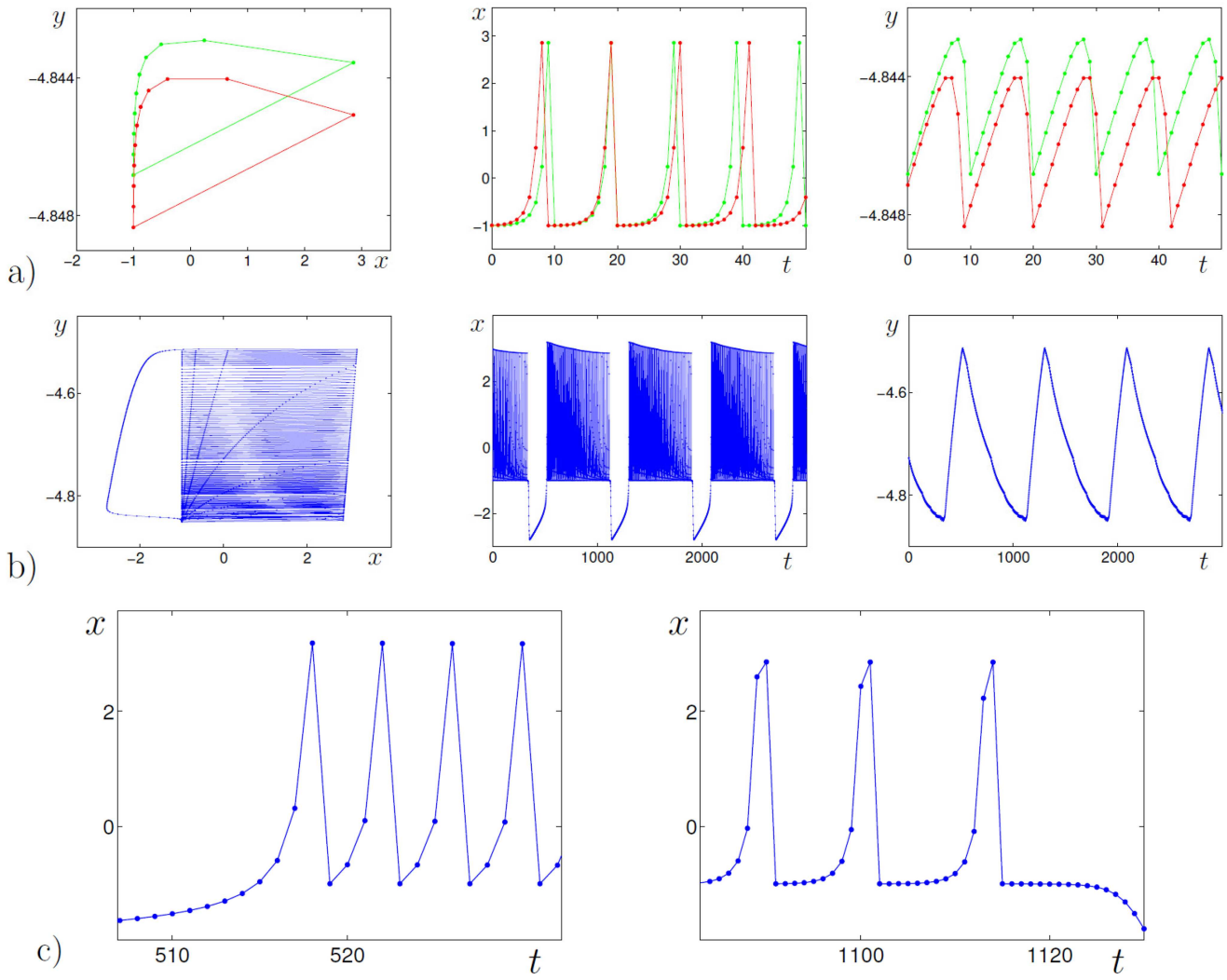

FIG. 3. Deterministic system (1) with $\alpha = 7.7$: (a) tonic spiking with 10-cycle (red) and 11-cycle (blue), (b) bursting, and (c) initial and final fragments of the burst.

where ξ_t are uncorrelated white Gaussian noises with parameters $\mathrm{E}(\xi_t) = 0$, $\mathrm{E}(\xi_t^2) = 1$, and ε is the noise intensity. In numerical simulations of Gaussian random disturbances, we used the Box–Muller algorithm.

A. Noise-induced transitions and dominants in the zone of coexisting cycles

First, consider how noise affects the 18-cycle in the stochastic system (2) with $\alpha = 2$ [see the upper cycle in Fig. 2(a)]. In Fig. 4(a), we plot deterministic 18-cycle (green) and 19-cycle (light blue) of system (1) with $\alpha = 2$. The random trajectory of system (2) with $\varepsilon = 3 \times 10^{-6}$ starting from the deterministic 18-cycle is plotted by blue color. As can be seen, under the random disturbances, this trajectory transits from 18-cycle to 19-cycle. Corresponding time series are shown by blue color in Fig. 4(b). In this figure, we also plot by gray the time series of the deterministic 18-cycle (upper) and 41-cycle (lower).

Under increasing noise, random trajectories, jumping from one cycle to another, stabilize near the lower cycles. A general statistical description of these transitions is summarized in Fig. 4(c) where finite-time mean values $m_y = \frac{1}{n}\sum_{i=1}^{n} y_i$ of y-coordinates of system (2) solutions starting from all coexisting deterministic cycles are plotted for $n = 10^6$ vs noise intensity ε. As can be seen, under increasing noise, solutions starting from upper cycles move downward whereas solutions starting from lower cycles move upward, and as a result of such transitions, mean values m_y stabilize for $\varepsilon > 1 \times 10^{-4}$.

The stochastic phenomenon of noise-induced shifts, shown here for $\alpha = 2$, is common for the entire α-zone of multi-rhythmicity.

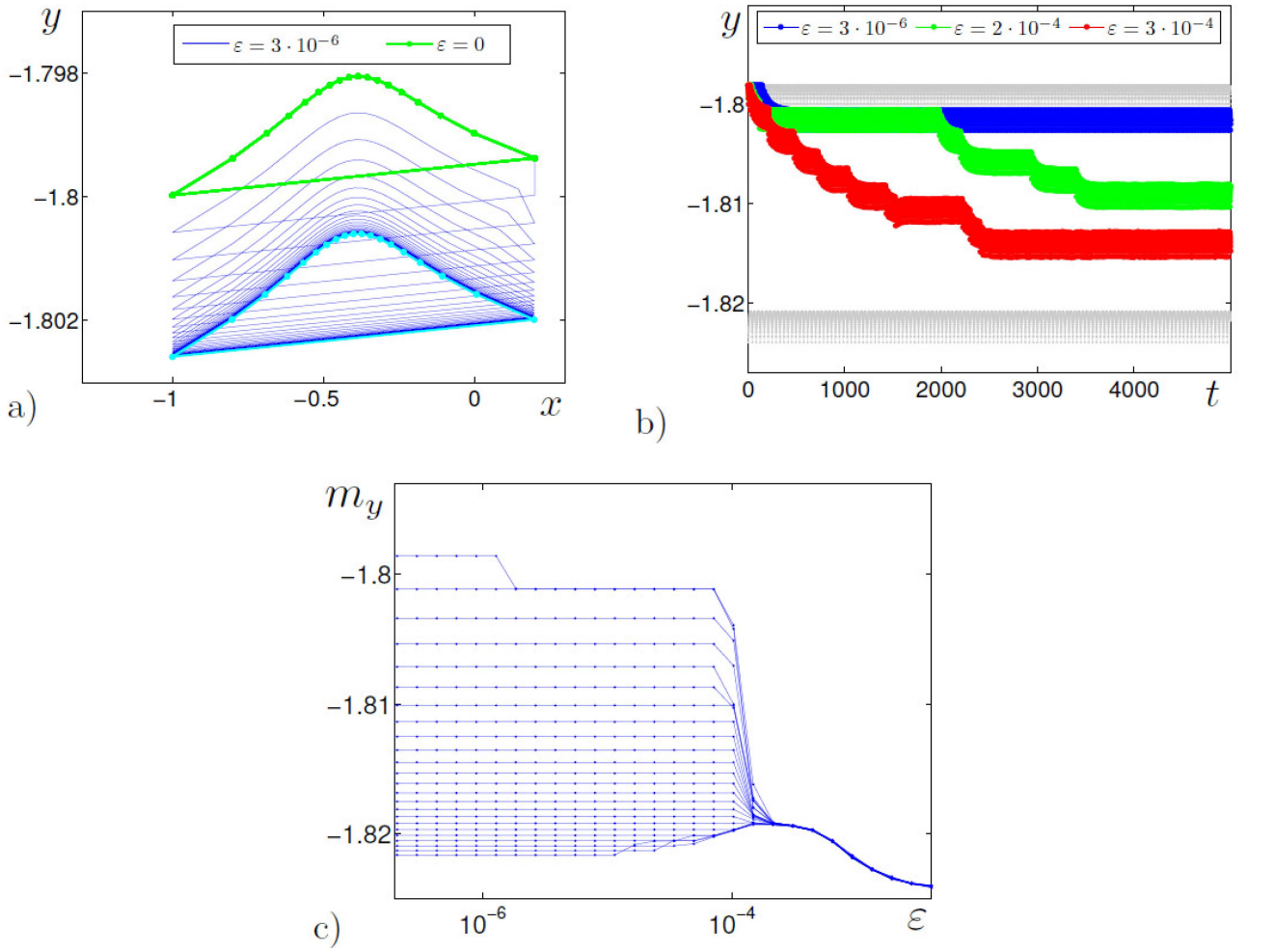

FIG. 4. Multi-stage noise-induced transitions between limit cycles in system (2) with $\alpha = 2$: (a) phase trajectories; (b) time series; and (c) mean values m_y of solutions vs noise intensity ε.

This is illustrated in Fig. 5 for $\alpha = 3$, $\alpha = 7$, and $\alpha = 7.5$. Here, along with shifts of mean values m_y (left column), we show shifts of mean values m_τ of interspike intervals τ (right column). In these stochastic transitions between coexisting cycles of different periods, the noise-induced "preference" is well seen. Indeed, for $\alpha = 3$, the increasing noise leads to the fact that the 11-cycle becomes dominant. For $\alpha = 7$, the 11-cycle is dominant as well. For $\alpha = 7.5$, noise "prefers" the 10-cycle.

In the analysis of mechanisms of noise-induced transitions between coexisting cycles, it is important to take into account the geometry of basins of attraction and their borders (separatrices). Indeed, for weak noise, random trajectories slightly deviate from the initial deterministic attractor and localize inside its basin of attraction. As the noise increases, the random trajectory can cross the separatrix and then be located near the neighboring attractor. Along with the geometry of basins of attraction, the stochastic sensitivity of attractors plays an important role in understanding the probabilistic mechanisms of noise-induced transitions.

Let us discuss how stochastic analysis of the aforementioned phenomena can be carried out. Here, as a conceptual example, we consider noise-induced transitions in the stochastic system (2) with $\alpha = 3$ (see Fig. 6). For $\alpha = 3$, the deterministic system possesses five coexisting cycles with periods 8, 9, 10, 11, and 12. Phase trajectories of these cycles are shown in Fig. 2(b). Basins B_8, B_9, B_{10}, B_{11}, and B_{12} of attraction of these coexisting cycles are presented in Fig. 6(a) by different colors. Deterministic 8-cycle (blue), 9-cycle (brown), and 10-cycle (pink) are plotted in Fig. 6(b). Here, we also indicate points M_i of the 8-cycle and show a stochastic trajectory starting from this 8-cycle for the noise intensity $\varepsilon = 2 \times 10^{-4}$. As can be seen, this trajectory transits from basin B_8 to basin B_9 and localizes near the 9-cycle. In Fig. 6(c), a time series of the deterministic 8-cycle are shown

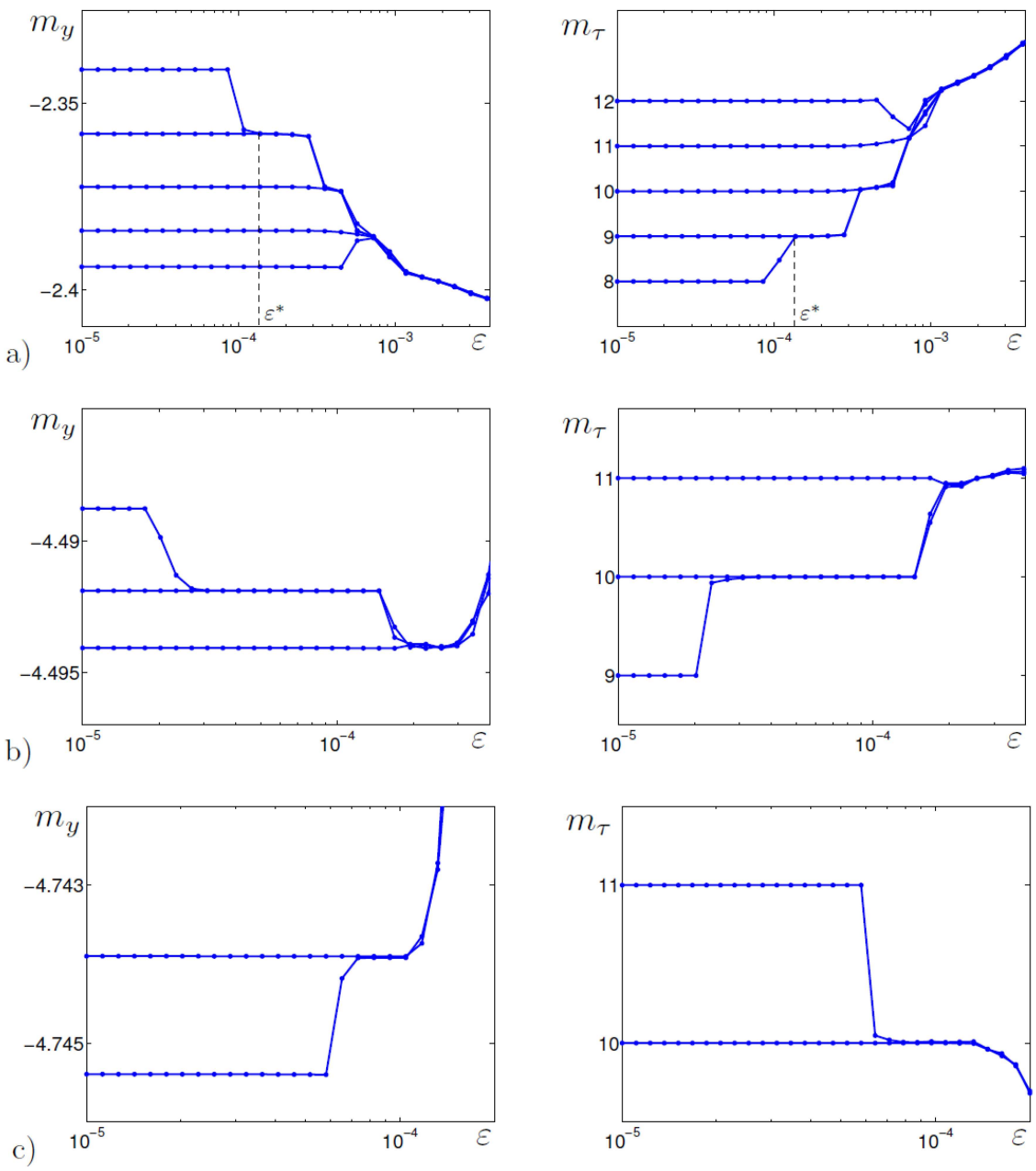

FIG. 5. Noise-induced shifts in stochastic system (2) with (a) $\alpha = 3$, (b) $\alpha = 7$, and (c) $\alpha = 7.5$. Left column: mean values m_y of solutions and right column: mean values m_τ of interspike intervals.

by blue; for the deterministic 9-cycle, they are plotted by brown; and the stochastic trajectory, which transits from 8-cycle to 9-cycle, is shown by light blue.

It should be noted that for smaller noise with intensity $\varepsilon = 5 \times 10^{-5}$, the random trajectory remains near 8-cycle. It is confirmed by statistics of interspike intervals [see Fig. 5(a), right].

Stochastic sensitivity of the deterministic 8-cycle $\{M_1, M_2, \ldots, M_8\}$ is characterized by the set of matrices $\{W_1, W_2, \ldots, W_8\}$. Mathematical details of the stochastic sensitivity theory of the cycles of discrete-time systems are given in Refs. 40 and 41. Applications of this theory to the analysis of various noise-induced phenomena can be found in Refs. 19 and 20.

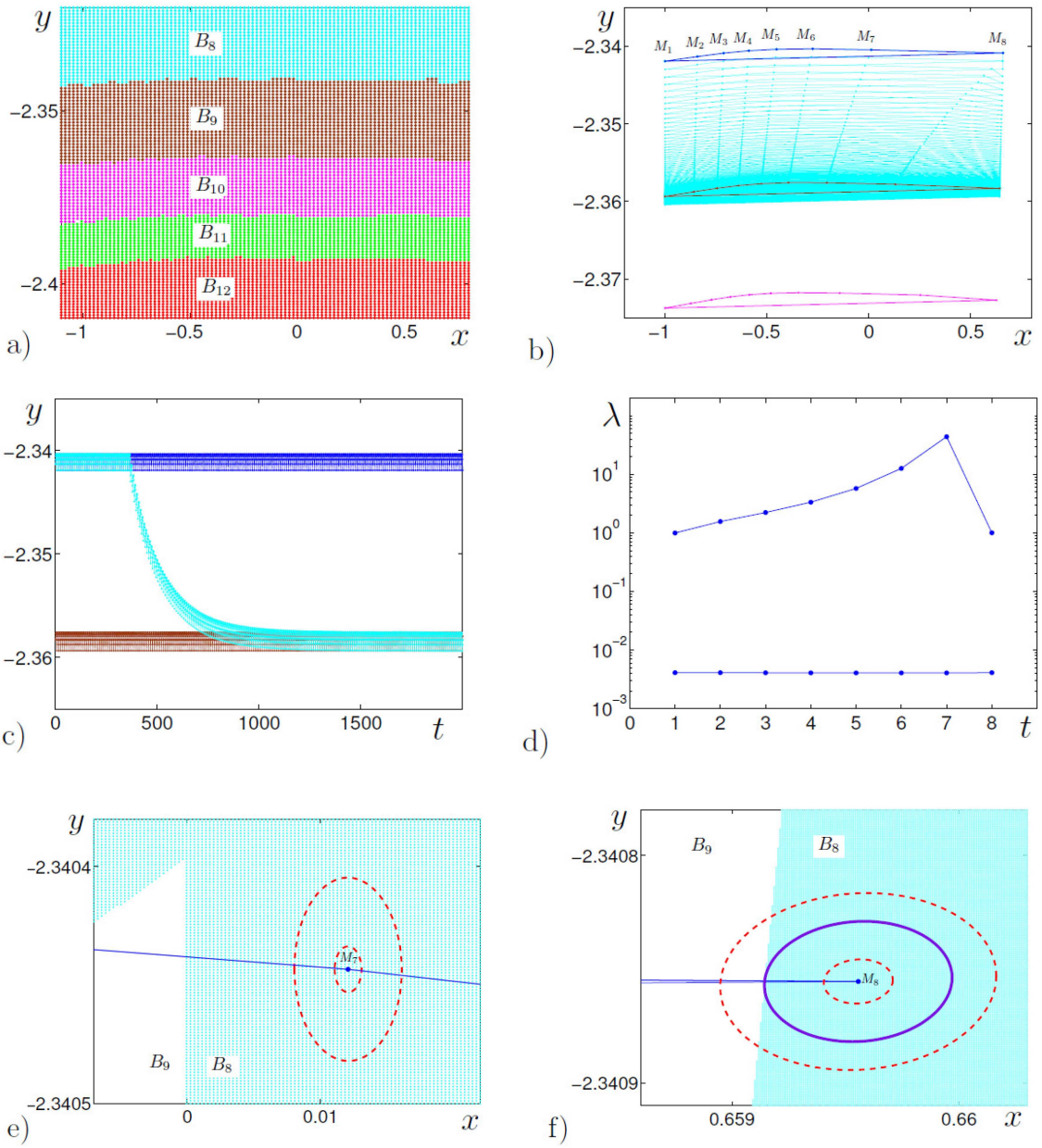

FIG. 6. Noise-induced transitions in system (2) with $\alpha = 3$: (a) basins B_8, B_9, B_{10}, B_{11}, and B_{12} of attraction for coexisting cycles with periods 8, 9, 10, 11, and 12; (b) and (c) transition of stochastic trajectory (light blue) from the 8-cycle (blue) to the 9-cycle (brown); (d) eigenvalues of stochastic sensitivity matrices $\{W_1, W_2, \ldots, W_8\}$ of the points $\{M_1, M_2, \ldots, M_8\}$ of 8-cycle; (e) and (f) basins of attraction B_8 (light blue) and B_9 (white) of 8- and 9-cycles, and confidence ellipses for $\varepsilon = 5 \times 10^{-5}$ (small dashed), $\varepsilon = 2 \times 10^{-4}$ (large dashed) around points M_7 and M_8. In (f), the confidence ellipse for the critical noise intensity $\varepsilon^* = 1.36 \times 10^{-4}$ is shown by the violet solid line.

Using eigenvalues λ_1, λ_2 and orthonormal eigenvectors v_1, v_2 of the stochastic sensitivity matrix W_t, one can construct a confidence ellipse around the point $M_t(\bar{x}_t, \bar{y}_t)$ of the considered 8-cycle,

$$\frac{z_1^2}{\lambda_1} + \frac{z_2^2}{\lambda_2} = -2\varepsilon^2 \ln(1 - P).$$

Here, z_1 and z_2 are coordinates of the ellipse on the basis of eigenvectors v_1, v_2 with the origin at the point M_t, and P is the fiducial probability. In Fig. 6(d), eigenvalues of matrices $\{W_1, W_2, \ldots, W_8\}$ are plotted. As can be seen, these eigenvalues differ in order, and the stochastic sensitivity significantly changes from one point of the cycle to another one.

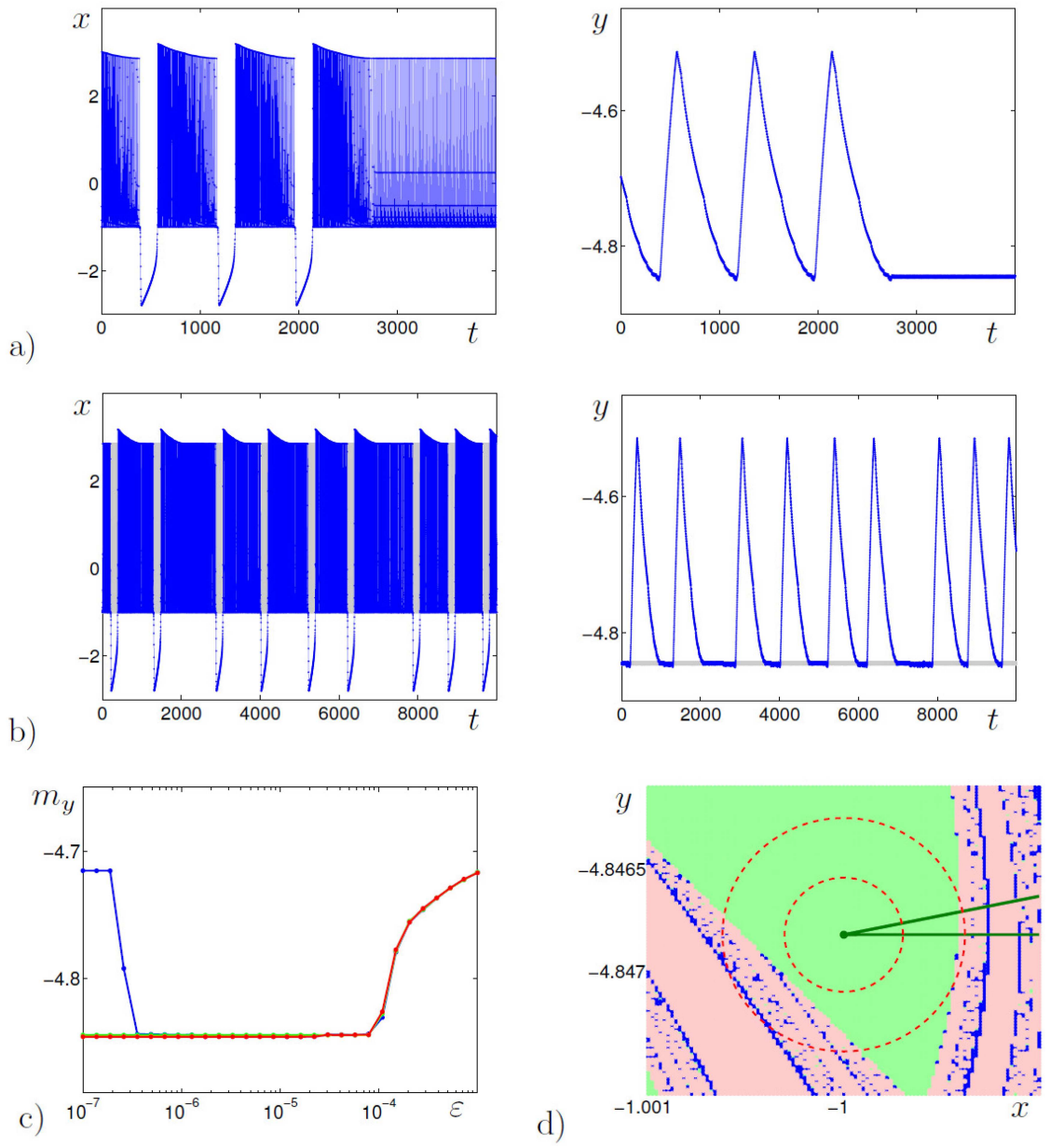

FIG. 7. Noise-induced transitions in system (2) with $\alpha = 7.7$: (a) from bursting to noisy spiking for $\varepsilon = 1 \times 10^{-6}$, (b) from tonic spiking to noisy bursting for $\varepsilon = 2 \times 10^{-4}$. In (c), we show mean values m_y of solutions starting from bursting (blue), 10-cycle (green), and 11-cycle (red). In (d), we show basins of attraction of the bursting (blue), 10-cycle (green), 11-cycle (red), and confidence ellipses (dashed) for $\varepsilon = 1 \times 10^{-4}$ and $\varepsilon = 2 \times 10^{-4}$.

Analysis of noise-induced transitions from 8-cycle to 9-cycle reveals that random trajectories leave 8-cycle near the point M_8 [see the light-blue trajectory in Fig. 6(b)]. In Figs. 6(e) and 6(f), points M_7 and M_8 are shown along with the basins B_8 (light blue) and B_9 (white) of 8- and 9-cycles. Key information on the dispersion of random states near points M_7 and M_8 is presented by confidence ellipses (dashed curves). Here, the small ellipse corresponds to the noise intensity $\varepsilon = 5 \times 10^{-5}$ whereas the large ellipse is constructed for $\varepsilon = 2 \times 10^{-4}$.

Note that the stochastic sensitivity of M_7 is essentially higher than that for M_8 [see Fig. 6(d)] but both ellipses around M_7 totally belong to the basin B_8. As for M_8, the large ellipse corresponding to

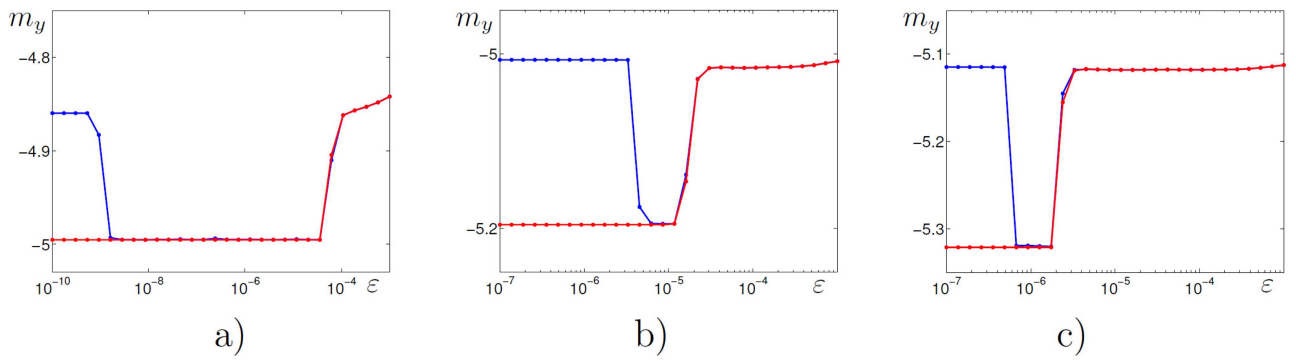

FIG. 8. Mean values m_y of solutions starting from the bursting (blue) and 10-cycle (red) for (a) $\alpha = 8$, (b) $\alpha = 8.4$, and (c) $\alpha = 8.65$.

$\varepsilon = 2 \times 10^{-4}$ partially occupies basin B_9. This fact signals the escape of the random trajectory from basin B_8 and the transition to B_9.

Thus, the analysis of the causes of transitions from one attractor to another requires studying not only the stochastic sensitivity of attractors but also the geometry of their basins of attraction. An intersection of the confidence ellipse with the separatrix between basins of attraction allows us to predict the onset of noise-induced transitions and estimate the corresponding critical value ε^*. In

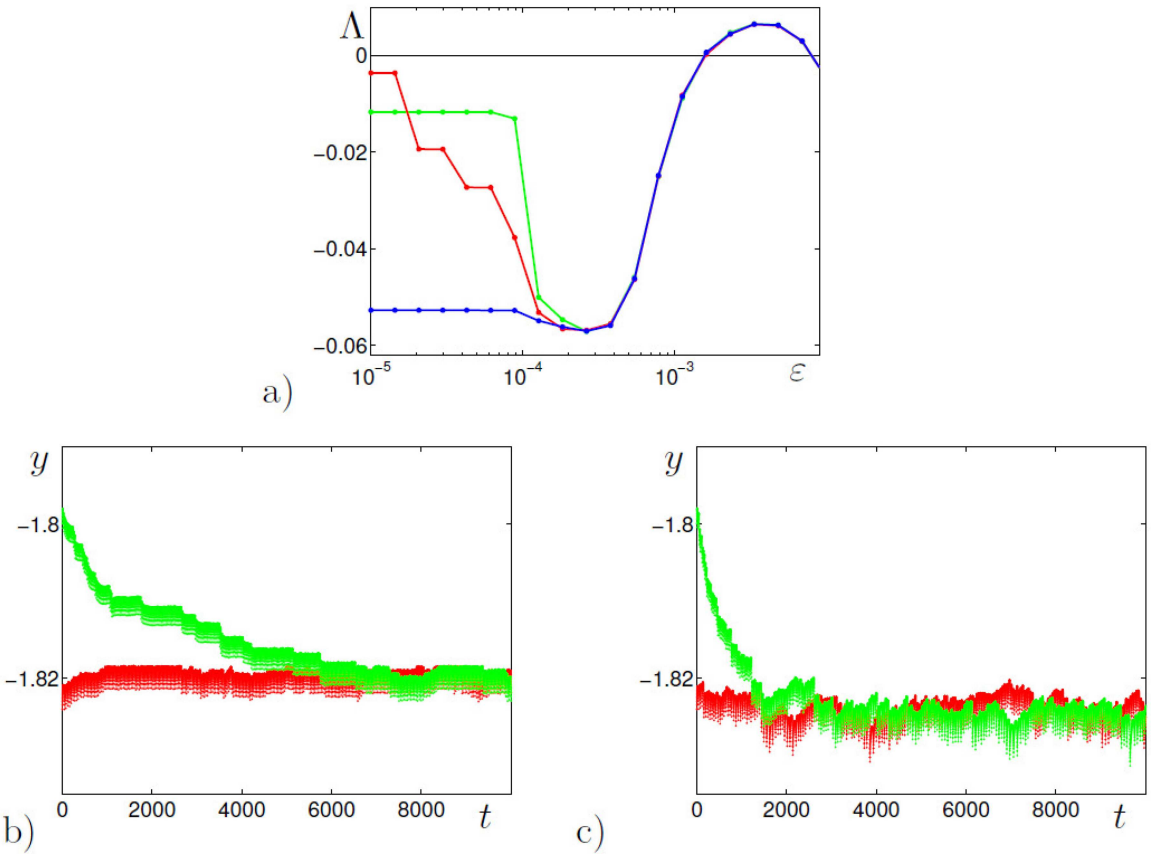

FIG. 9. Noise-induced chaos in system (2) with $\alpha = 2$: (a) largest Lyapunov exponents, (b) stochastic trajectories for $\varepsilon = 0.0003$, and (c) stochastic trajectories for $\varepsilon = 0.004$.

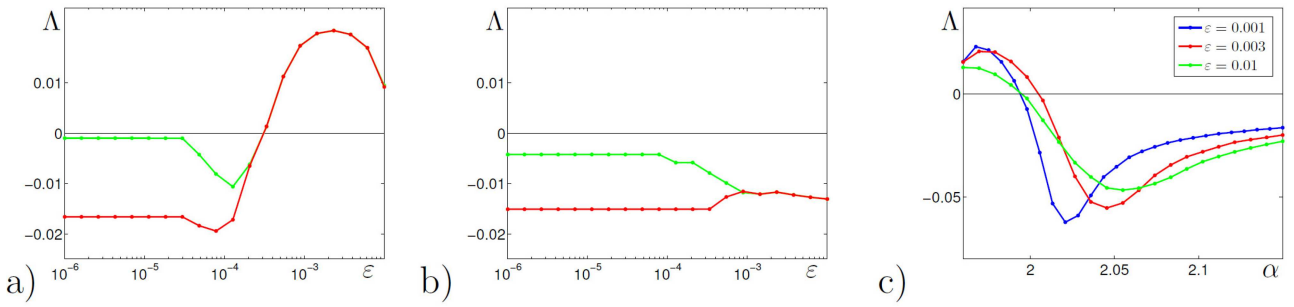

FIG. 10. Largest Lyapunov exponents of system (2) (a) for $\alpha = 1.98$, (b) for $\alpha = 3$, and (c) for different ε vs α.

Fig. 6(f), the confidence ellipse that touches the separatrix between basins B_8 and B_9 is shown by the violet solid line. This ellipse was calculated for $\varepsilon^* = 1.36 \times 10^{-4}$, playing the role of the critical noise intensity. The value ε^* is marked in Figs. 5(a) and 5(b). As can be seen, this theoretical estimation based on the stochastic sensitivity method well predicts the noise intensity at which noise-induced transitions from 8-cycle to 9-cycle occurs.

B. Noise-induced transformations in the zone of coexisting tonic spiking and bursting

Consider now stochastic effects in the parameter zone $\alpha > \alpha_2$ with more complex multi-rhythmicity where tonic spiking coexists with bursting-type attractors.

In Fig. 7, we present noise-induced phenomena in system (2) with $\alpha = 7.7$. For $\alpha = 7.7$, the deterministic system has three coexisting attractors: 10-cycle (green), 11-cycle (red), and bursting attractor (blue) shown in Fig. 3. In Fig. 7(a), a time series of solutions of system (2) with $\varepsilon = 1 \times 10^{-6}$ starting from the bursting attractor are plotted. As one can see, these random solutions transit from the bursting regime to the spiking one. So, here, extremely weak noise suppresses bursting.

In Fig. 7(b), a time series of the deterministic 10-cycle are shown by gray, and a time series of the stochastic system (2) with $\varepsilon = 2 \times 10^{-4}$ starting from this 10-cycle are plotted by blue. Here, we observe mutual transitions between 10-cycle and bursting attractor. So, for $\varepsilon = 2 \times 10^{-4}$, the generation of noisy bursting occurs.

Details of the transformation of dynamics under increasing ε are shown in Fig. 7(c), where mean values of y-coordinates of solutions starting from bursting (blue), 10-cycle (green), and 11-cycle (red) are presented. As can be seen, stochastic dynamics undergoes three stages of deformation. First, noise suppresses bursting with the transition "bursting → 10-cycle." The second stage is the transition "11-cycle → 10-cycle." The final stage is the transformation of the noisy 10-cycle to the noisy bursting.

Critical noise intensity corresponding to the third stage can be estimated by the confidence ellipses. In Fig. 7(d), we show basins of attraction of the bursting (blue), 10-cycle (green), and 11-cycle (red) near the point (−1,−4.846 82) of the 10-cycle (dark green). Here, confidence ellipses (dashed) are plotted for $\varepsilon = 1 \times 10^{-4}$ and $\varepsilon = 2 \times 10^{-4}$. A small ellipse totally belongs to the basin of 10-cycle whereas the large ellipse partially occupies the basin of the bursting attractor. This arrangement predicts the noise-induced generation of the bursting for $\varepsilon = 2 \times 10^{-4}$ that agrees with the results of the direct numerical simulation shown in Fig. 7(c).

With the further increase of α, system (1) becomes bistable with coexisting bursting attractor and 10-cycle. For such a bistability zone, noise-induced transitions are illustrated in Fig. 8 for $\alpha = 8$, $\alpha = 8.4$, and $\alpha = 8.65$ by mean values m_y vs noise intensity. These plots are shown for solutions starting from the bursting attractor by blue and from the 10-cycle by red. As can be seen, noise deforms system dynamics and causes transitions between bursting and spiking.

C. Lyapunov exponents and noise-induced chaos

Consider now how noise, which causes stochastic spatial and frequency deformations of oscillatory regimes, discussed above, changes Lyapunov exponents. A sign of the largest Lyapunov exponent Λ defines a key intrinsic dynamical property: its positiveness/negativeness means a divergence/convergence of system solutions. A change of the sign of the Λ from minus to plus is a known criterion of the transition from order to chaos.[31]

In Fig. 9(a), three branches of the function $\Lambda(\varepsilon)$ are shown for $\alpha = 2$. The green curve was calculated for random solutions starting from the 18-cycle, the blue curve for random solutions starting from the 31-cycle, and the red curve for solutions starting from the 41-cycle [see deterministic cycles in Fig. 2(a)].

For weak noise, when random trajectories are located near the initial attractors, the branches of the function $\Lambda(\varepsilon)$ are well separated. With increasing noise, because of transitions from one cycle to another and the further merging of stochastic distributions near 31-cycle [compare with Fig. 4(c)], red and green branches of the $\Lambda(\varepsilon)$ decrease and join with blue branch corresponding to 31-cycle. This can be interpreted as noise-induced stabilization of the system (2).

With a further increase of ε, the frequency of transitions between basins of coexisting deterministic cycles grows, and the system begins by spending more time near separatrices, in the zones with high local divergence. As a result, function $\Lambda(\varepsilon)$ begins to grow and becomes positive. This effect can be interpreted as noise-induced chaos. To illustrate these phenomena, we show time series in Figs. 9(b) and 9(c).

Some additional features of noise-induced "order–chaos" transformations in dependence on the variation of parameters ε and

α are presented in Fig. 10. For $\alpha = 1.98$ [see Fig. 10(a)] that is closer to the bifurcation value α_1, the onset of chaos occurs for the smaller values of ε in comparison with $\alpha = 2$. For $\alpha = 3$ that is farther from α_1, chaos is not observed [see Fig. 10(b)]. For three values of the parameter ε, detailed dependence of Λ on α is shown in Fig. 10(c). Here, α-parameter zones of chaos and order are well seen.

IV. CONCLUSION

We considered a multirhythmic map-based model of the neuron activity under random disturbances. Our study focused on the parameter zone where diverse oscillatory regimes coexist: spiking cycles with various periods and bursts. A probabilistic mechanism of noise-induced transition from one rhythm to another is studied. Here, along with statistics extracted from direct numerical simulation, we analyzed the stochastic sensitivity of periodic attractors and spatial peculiarities of their basins. Based on the apparatus of confidence ellipses, we estimated the strength of noise that induces transitions from one basin to another. We revealed some kind of "stochastic preference" in these transitions between cycles and showed that these transitions are accompanied by order–chaos transformations.

ACKNOWLEDGMENTS

This work was supported by the Russian Science Foundation (No. 21-11-00062).

DATA AVAILABILITY

The data that support the findings of this study are available from the corresponding author upon reasonable request.

REFERENCES

[1]G. B. Ermentrout and D. H. Terman, *Mathematical Foundations of Neuroscience* (Springer-Verlag, New York, 2010).
[2]E. M. Izhikevich, *Dynamical Systems in Neuroscience: The Geometry of Excitability and Bursting* (MIT Press, Cambridge, 2007).
[3]E. M. Izhikevich, "Neural excitability, spiking and bursting," Int. J. Bifurcation Chaos **10**(6), 1171–1266 (2000).
[4]R. FitzHugh, "Impulses and physiological states in theoretical models of nerve membrane," Biophys. J. **1**(6), 445–466 (1961).
[5]A. S. Pikovsky and J. Kurths, "Coherence resonance in a noise-driven excitable system," Phys. Rev. Lett. **78**(5), 775–778 (1997).
[6]I. Bashkirtseva, L. Ryashko, and E. Slepukhina, "Noise-induced oscillation bistability and transition to chaos in FitzHugh–Nagumo model," Fluctuation Noise Lett. **13**(1), 1450004 (2014).
[7]C. Morris and H. Lecar, "Voltage oscillations in the Barnacle giant muscle fiber," Biophys. J. **35**, 193–213 (1981).
[8]J. L. Hindmarsh and R. M. Rose, "A model of neuronal bursting using three coupled first order differential equations," Proc. R. Soc. London, Ser. B **221**(1222), 87–102 (1984).
[9]A. Shilnikov and M. Kolomiets, "Methods of the qualitative theory for the Hindmarsh–Rose model: A case study—A tutorial," Int. J. Bifurcation Chaos **18**(8), 2141–2168 (2008).
[10]I. Bashkirtseva, L. Ryashko, and E. Slepukhina, "Order and chaos in the stochastic Hindmarsh–Rose model of the neuron bursting," Nonlinear Dyn. **82**(1), 919–932 (2015).
[11]A. L. Hodgkin and A. F. Huxley, "A quantitative description of membrane current and its application to conduction and excitation in nerve," J. Physiol. **117**, 500–544 (1952).
[12]C. Zhou and J. Kurths, "Noise-induced synchronization and coherence resonance of a Hodgkin–Huxley model of thermally sensitive neurons," Chaos **13**, 401–409 (2003).
[13]I. Bashkirtseva and L. Ryashko, "Stochastic sensitivity and method of principal directions in excitability analysis of the Hodgkin–Huxley model," Int. J. Bifurcation Chaos **29**, 1950186 (2019).
[14]N. F. Rulkov, "Modeling of spiking–bursting neural behavior using two-dimensional map," Phys. Rev. E **65**, 041922 (2002).
[15]A. L. Shilnikov and N. F. Rulkov, "Origin of chaos in a two-dimensional map modeling spiking–bursting neural activity," Int. J. Bifurcation Chaos **13**, 3325–3340 (2003).
[16]M. Courbage and V. I. Nekorkin, "Map based models in neurodynamics," Int. J. Bifurcation Chaos **20**, 1631–1651 (2010).
[17]B. Ibarz, J. M. Casado, and M. A. F. Sanjuán, "Map-based models in neuronal dynamics," Phys. Rep. **501**, 1–74 (2011).
[18]I. Bashkirtseva, V. Nasyrova, and L. Ryashko, "Noise-induced bursting and chaos in the two-dimensional Rulkov model," Chaos, Solitons Fractals **110**, 76–81 (2018).
[19]I. Bashkirtseva, V. Nasyrova, and L. Ryashko, "Analysis of noise effects in a map-based neuron model with Canard-type quasiperiodic oscillations," Commun. Nonlinear Sci. Numer. Simul. **63**, 261–270 (2018).
[20]I. Bashkirtseva, V. Nasyrova, and L. Ryashko, "Stochastic spiking–bursting excitability and transition to chaos in a discrete-time neuron model," Int. J. Bifurcation Chaos **30**(10), 2050153 (2020).
[21]B. Ibarz, J. M. Casado, and M. A. F. Sanjuán, "Patterns in inhibitory networks of simple map neurons," Phys. Rev. E **75**, 041911 (2007).
[22]I. Franovic and V. Miljkovic, "The effects of synaptic time delay on motifs of chemically coupled Rulkov model neurons," Commun. Nonlinear Sci. Numer. Simul. **16**, 623–633 (2011).
[23]C. Wang and H. Cao, "Stability and chaos of Rulkov map-based neuron network with electrical synapse," Commun. Nonlinear Sci. Numer. Simul. **20**, 536–545 (2015).
[24]P. Ge and H. Cao, "Synchronization of Rulkov neuron networks coupled by excitatory and inhibitory chemical synapses," Chaos **29**, 023129 (2019).
[25]E. Rybalova, A. Bukh, G. Strelkova, and V. Anishchenko, "Spiral and target wave chimeras in a 2D lattice of map-based neuron models," Chaos **29**(10), 101104 (2019).
[26]A. N. Pisarchik and U. Feudel, "Control of multistability," Phys. Rep. **540**, 167–218 (2014).
[27]V. S. Anishchenko, V. V. Astakhov, A. B. Neiman, T. E. Vadivasova, and L. Schimansky-Geier, *Nonlinear Dynamics of Chaotic and Stochastic Systems. Tutorial and Modern Development* (Springer-Verlag, Berlin, 2007).
[28]C. Laing and G. J. Lord, *Stochastic Methods in Neuroscience* (Oxford University Press, 2009).
[29]M. D. McDonnell, N. G. Stocks, C. E. M. Pearce, and D. Abbott, *Stochastic Resonance: From Suprathreshold Stochastic Resonance to Stochastic Signal Quantization* (Cambridge University Press, 2008).
[30]W. Horsthemke and R. Lefever, *Noise-Induced Transitions* (Springer, Berlin, 1984).
[31]J. B. Gao, S. K. Hwang, and J. M. Liu, "When can noise induce chaos?," Phys. Rev. Lett. **82**(6), 1132–1135 (1999).
[32]B. Lindner, J. Garcia-Ojalvo, A. Neiman, and L. Schimansky-Geier, "Effects of noise in excitable systems," Phys. Rep. **392**, 321–424 (2004).
[33]V. A. Makarov, V. I. Nekorkin, and M. G. Velarde, "Spiking behavior in a noise-driven system combining oscillatory and excitatory properties," Phys. Rev. Lett. **86**(15), 3431–3434 (2001).
[34]T. Nagy, E. Verner, V. Gaspar, H. Kori, and I. Z. Kiss, "Delayed feedback induced multirhythmicity in the oscillatory electrodissolution of copper," Chaos **25**, 064608 (2015).
[35]D. Biswas, T. Banerjee, and J. Kurths, "Control of birhythmicity through conjugate self-feedback: Theory and experiment," Phys. Rev. E **94**, 042226 (2016).
[36]A. Tosolini, M. Patzauer, and K. Krischer, "Bichaoticity induced by inherent birhythmicity during the oscillatory electrodissolution of silicon," Chaos **29**, 043127 (2019).

[37]T. Haberichter, M. Marhl, and R. Heinrich, "Birhythmicity, trirhythmicity and chaos in bursting calcium oscillations," Biophys. Chem. **90**, 17–30 (2001).
[38]J. Yan and A. Goldbeter, "Multi-rhythmicity generated by coupling two cellular rhythms," J. R. Soc. Interface **16**, 20180835 (2019).
[39]I. Bashkirtseva, L. Ryashko, and S. Zaitseva, "Stochastic sensitivity analysis of noise-induced transitions in a biochemical model with birhythmicity," J. Phys. A: Math. Theor. **53**, 265601 (2020).
[40]I. Bashkirtseva, L. Ryashko, and I. Tsvetkov, "Sensitivity analysis of stochastic equilibria and cycles for the discrete dynamic systems," Dyn. Contin. Discrete Impulsive Syst. Ser. A: Math. Anal. **17**, 501–515 (2010).
[41]I. Bashkirtseva and L. Ryashko, "Stochastic deformations of coupling-induced oscillatory regimes in a system of two logistic maps," Physica D **411**, 132589 (2020).